8CUEE CONFERENCE PROCEEDINGS
8th International Conference on Urban Earthquake Engineering
March 7-8, 2011, Tokyo Institute of Technology, Tokyo, Japan

FUNDAMENTAL STUDY ON PROBABILISTIC EVALUATION OF THE ULTIMATE STATE OF BASE ISOLATED STRUCTURES

Toshiyuki Nakazawa[1], Shoichi Kishiki[2], Zhe Qu[3], Arata Miyoshi[4], and Akira Wada[5]

1) Tokyo-Kenchiku Structural Engineering, Japan
2) Assistant professor, Structural Engineering Research Center, Tokyo Institute of Technology, Japan
3) Postdoctoral research fellow, Center for Urban Earthquake Engineering, Tokyo Institute of Technology, Japan
4) Graduate student, Tokyo Institute of Technology, Japan
5) Professor, Structural Engineering Research Center, Tokyo Institute of Technology, Japan
nakazawa-t@tkse2000.co.jp, kishiki@serc.titech.ac.jp, m.quzhe@gmail.com, miyoshi.a.aa@m.titech.ac.jp, wada@serc.titech.ac.jp

Abstract: Seismic base isolation is effective to control the seismic responses of building structures. However, compared with conventional seismic systems, the robustness of the base-isolated buildings is generally considered lower and thus the selection of input ground motions becomes a more crucial issue in assessing the seismic safety of base-isolated buildings. Extensive incremental dynamic analysis (IDA) is carried out to evaluate the ultimate state of base isolated buildings in terms of the fragility curves. The ground motion record set in FEMA P695 is adopted for analysis. The influences of the stiffness of isolation layer, the height of rubber bearings, clearance and hysteretic behavior of the retaining walls as well as the strength of the superstructures are examined. Based on the analysis results, the following can be concluded:(1) increasing the clearance of retaining walls is the most effective manner to enhance the seismic safety of base isolated buildings; (2) the seismic safety margin of base-isolated buildings might be significantly increased with stronger superstructures only if the retaining wall is appropriately proportioned so that the yielding of retaining wall is prior to that of the superstructure.

1. INTRODUCTION

The deformation pattern of base-isolated structures is clearly defined by employing a soft isolation layer at the bottom of the building, which is usually composed of both isolators and energy dissipating devices. Under earthquakes, most deformations and energy dissipations are expected to concentrate in the isolation layer so that the superstructure suffers only slight damage. But on the other hand, the robustness of isolated structures subjected to unexpected violent earthquakes remains questionable (Kikuchi *et al*, 1995). Shaking table test reveals that reinforced concrete walls in the superstructure of isolated structures are likely to suffer severe damage if hardening of the rubber bearing in the isolation layer occurs (Kitamura *et al*, 2009).

In order to assess the seismic safety of base-isolated structures under unexpected earthquakes, the incremental dynamic analysis proposed by Vamvatsikos *et al* (2002) is employed and the collapse margin ratios (CMR) of base-isolated structures with various parameters are evaluated in accordance with the framework in FEAM P695 (2009). The following ultimate states are considered in this study: (1) hardening and fracture of rubber bearing; (2) collision of the superstructure with surrounding retaining walls; (3) excessive damage in the superstructures. The failure of dampers is not considered.

2. ANALYSIS MODEL

The base-isolated structure is modeled by a 2-DOF system as shown in Figure 1. The weight of superstructure and isolation layer is 150,000kN and 40,000kN, respectively. Hysteretic behavior of each component is introduced below.

2.1 Superstructure

The superstructure is modeled by a SDOF system with tri-linear degrading hysteresis (Takeda *et al*, 1970) as shown in Figure 1(a). Yield strength Q_y is set to be base shear coefficient C_0 times the superstructure weight W_S (150,000kN). Cracking strength is $0.3Q_y$ and the secant stiffness at yielding point is 0.3 times the initial stiffness. Post-yielding tangent stiffness is 0.001 times the initial stiffness. Unloading stiffness ratio β=0.4. Damping of the superstructure is assumed proportional to the tangent stiffness with a 2% damping ratio at the fixed-base period. For non-isolated structure, 3% damping ratio is assumed to consider the damping induced by soil-structure interaction.

In this study, C_0 varies from 0.15 to 0.40 with an increment of 0.05. The initial stiffness is assumed to be proportional with C_0 value. In the case of C_0=0.3, which is a common practice in Japan, the fundamental period of fixed-base structure is assumed to be 0.3s, and the

corresponding initial stiffness is $6{,}709 \times 10^3$kN/m.

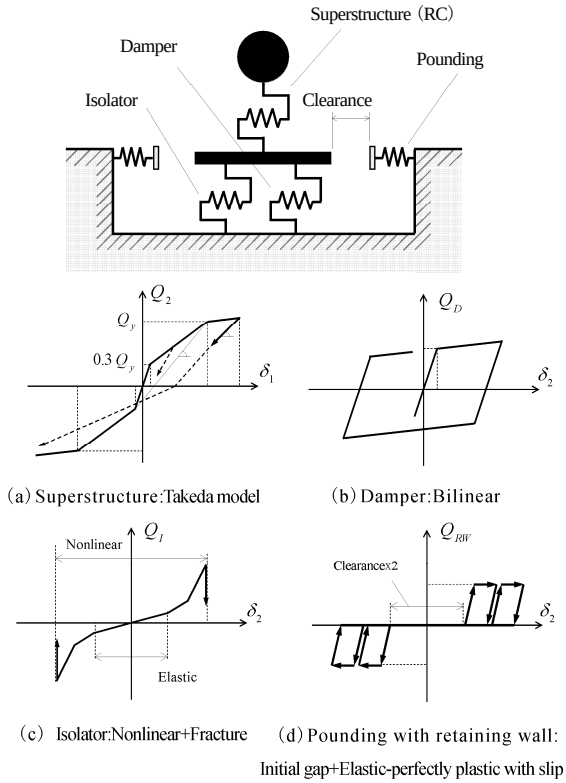

Figure 1　Analysis model and the hysteretic behavior

2.2　Damper

It is assumed that the damper have adequate deformation capacity up to the collapse of the structure. Bilinear hysteretic behavior with an initial stiffness of 240.0×10^3kN/m and a post-yielding stiffness ratio of 1/60 is assumed for the damper (Figure 1b). The damper yield strength is 7,600kN, which is 0.04 times the total weight of the whole structure.

2.3　Isolator

It is assumed that natural rubber bearing is used as seismic isolator. Nonlinear elastic behavior with deformation limit as shown in Figure 1(c) is assumed. The initial stiffness k_{i1} is determined by tuning the isolation period T_f (Equation 1) to 4.0s, 5.0s and 6.0s. The corresponding k_{i1} is 47800, 30600 and 21300kN/m, respectively.

$$T_f = 2\pi\sqrt{M/k_{i1}} \tag{1}$$

where M is the total weight of the structure.

It is assumed that the tangent stiffness of the isolator increases to $k_{i2}=2k_{i1}$ in the shear strain range of 250%~350%, and $k_{i3}=7.0k_{i1}$ in the range of 350%~450%. Shear strain of 450% defines the ultimate deformation of the isolator. These assumptions are made based on the test results reported in previous studies (Takayama, 1995; Yabana *et al*, 1996; Uryu *et al*, 1996; JSI, 1995). The isolator fracture deformation can be adjusted by varying the total rubber thickness nt_R. In this study, nt_R varies from 160mm, 200mm to 240mm. The corresponding fracture deformations of the isolator are 720mm, 900mm to 1080mm, respectively.

Beyond 450% shear strain, the isolator fractures and the restoring force is replaced by the friction between the isolation layer and its foundation. This is modeled by an elastic-perfectly plastic behavior with an elastic stiffness of 1600~3600 times the isolator stiffness and a strength of 0.4 times the total weight of the structure. The fall down of the isolation layer due to isolator fracture is not considered.

2.4　Pounding with retaining wall

An elastic-perfectly plastic spring with slip and initial gap is used to model the retaining wall and the clearance to the superstructure (Figure 1d). The same retaining wall as used by Kashiwa *et al* (2005) is assumed. Elastic stiffness is 57.5×10^3kN/m and the yield strength is 34,500kN. The clearance varies from 500mm, 800mm to infinity (no pounding).

3.　GROUND MOTIONS

A set of strong ground motions representing an earthquake scenario is required when evaluating the seismic performance using the incremental dynamic analysis. In this study, the selection of ground motion records is based on the Far-Field set in FEMA P695 (2009). Among the 22 records in the Far-Filed set, 8 components from 6 records are considered not appropriate for evaluating the seismic performance of seismic isolated buildings in this study since their lowest usable frequencies are no less than 0.167Hz, which indicates the long period contents with period longer than 6.0s are not reliable. For this reason, these 6 records are removed from the record set and only the remaining 16 records are used in this study.

3.1　Normalization of ground motion records

In order to remove the unwarranted variability in the ground motions, the selected records should be appropriately normalized. In FEMA P695, the records are normalized by the geometric mean of the peak ground velocities (PGV) of the two horizontal components. This method is dependent on the direction of observation.

In this study, each record is first rotated to the direction where the maximum PGV occurs. The ground acceleration in this direction is denoted as GA_{MV}, where the subscript MV stands for “Maximum Velocity”. The normalization factor is then calculated by Equation 2.

$$NM_i = \text{median}\left(PGV_{MV,i}\right)/PGV_{MV,i} \tag{2}$$

where PGV_{MV} is the PGV of GA_{MV}, the subscript i denotes the record number.

3.2　Scaling of record set

In an incremental dynamic analysis, the intensity of the scenario earthquake represented by the ground motion record set needs to be scaled incrementally until the ultimate

failure of the structure is achieved. Before doing so, some intensity measure (IM) needs to be defined. In FEMA P695, the median of the 5% damping spectral accelerations at the fundamental period $S_a(T_1, 5\%)$ of the record set is used as the IM. However, as recommended by Akiyama (1980), the equivalent velocity at the isolation period $V_E(T_f)$ can better represent the seismic response of base-isolated structures, which usually have long natural periods of vibration. T_f is given in Equation 1. The equivalent velocity V_E is a representation of the earthquake input energy with the unit of velocity. It is calculated by Equation 3.

$$V_E(T) = \sqrt{2E_I(T,10\%)/M} \quad (3)$$

where T is the natural period, $E_I(T, 10\%)$ is the input energy for a SDOF system with a period of T and 10% damping. M is the total mass of the system.

In this study, the median $V_E(T_f)$ of the normalized records is chosen to be the IM in the incremental dynamic analysis for base-isolated structure. For conventional non-isolated structures, the median $S_a(T_1)$ of the normalized records is used as the IM following FEMA P695. Note that the method of normalizing the records for both isolated and non-isolated structures is the same.

Since the IM for based-isolated and non-isolated structures are different, the intensity ratio (IR) defined as the ratio of the currently-used IM and design level IM is used to interpret the incremental dynamic analysis results (Equation 4).

$$\mathrm{IR} = \mathrm{IM}/\mathrm{IM}_D \quad (4)$$

IM_D is the design equivalent velocity $V_S(T_f)$ for base-isolated structures, and the design spectral acceleration $S_a(T_1)$ for non-isolated structures. $V_S(T_f)$ and $S_a(T_1)$ at the engineering bedrock recommended by BCJ (2005) are adopted. They can be easily transformed to those at other site conditions by multiplying the surface geology factor $G_s(T)$ recommended by BCJ (2005).

Figure 2 shows the equivalent velocity of the 16 ground motion records after being normalized and scaled to IR=1.0 for isolated structures with a period of 4.0s. Details of the selected ground motions are given in the appendix.

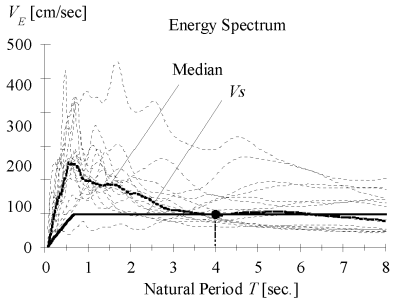

Figure 2 Equivalent velocity spectrum of normalized records when IR=1.0

4. INCREMENTAL DYNAMIC ANALYSIS

The IDA curves of the based-isolated structures with T_f=4.0s and C_0=0.3 as well as the corresponding non-isolated conventional structure are compared in Figure 3. In the IDA curves, the ductility of the superstructure defined as the ratio of the maximum and the yield deformation is chosen as the damage measure (DM).

For the based-isolated structure, 3 models denoted as Model A, B and C are used to examine the effect on the seismic performance of isolator fracture and pounding against the retaining wall. The 3 models are:

Model A. Ideal isolation. The isolator is assumed linearly elastic and no retaining wall is modeled (or the clearance is infinite).

Model B. The total rubber thickness of the isolator nt_R is 200mm and the hardening and fracture of the isolator as described above is considered. Still, no retaining wall is modeled.

Model C. Linearly elastic retaining wall with a 500mm clearance to the structure is modeled. All the other parameters are the same as in Model B.

Figure 3 gives the IDA curves for the non-isolated and the 3 models of the isolated structure. Dotted lines are the IDA curves for individual ground motions and bold solid lines mark the 16th, 50th (median) and 84th percentile of the IDA curves.

In terms of the median IDA curve, damages to the non-isolated structure increases gradually with the increase of intensity ratio (Figure 3a). No obvious softening of the median IDA curve can be observed since neither strength deterioration nor P-Δ effect are considered in the modeling, i.e. the structure does not exhibit negative stiffness.

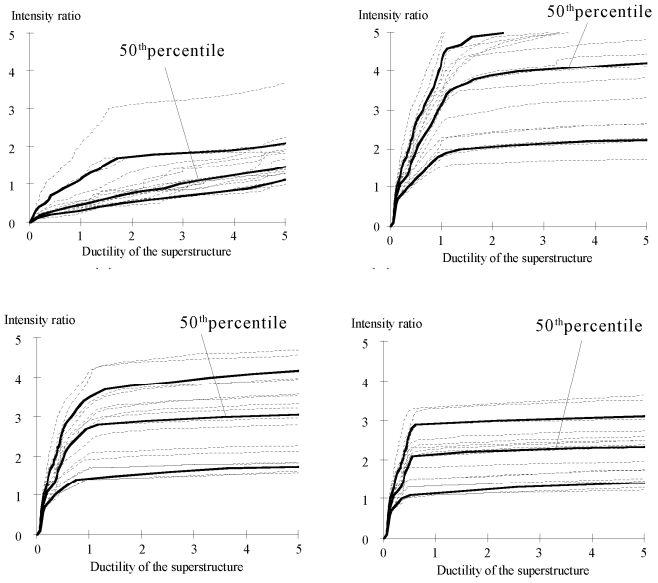

(c) Model B: Isolator fracture (d) Model C: Pounding

Figure 3 IDA curves of non-isolated and based-isolated structure

In contrast, the damage of the superstructure in the isolated building is limited to a very low level (say the ductility is below 1.0) prior to a certain limit of earthquake intensity. Beyond the limit, significant softening occurs even if the *P-Δ* effect is not considered. The superstructure ductility grows rapidly with slight increase of earthquake intensity.

From Figure 3(b)-(d), it is evident that the nonlinearity of the isolator and the pounding with the retaining wall significantly deteriorates the seismic performance of base-isolated structure. The value of IR when median IDA curve softens is about 4 for ideally isolated structure (Model A, Figure 3b). It is reduced to about 3 when nonlinearity of the isolator is considered (Model B, Figure 3c) and is further reduced to only about 2 if pounding occurs (Model C, Figure 3d).

It is also worth noting that the dispersions of IDA curves of isolated structures that can be visually identified by the range between 16th and 84th percentile in Figure 3(b)-(d) are also significantly reduced if the isolator's nonlinearity and the pounding are considered.

5. COLLAPSE MARGIN RATIOS

It is assumed herein that the structure or the superstructure in an isolated building collapses at the ductility of 4.0. The corresponding intensity ratios (IR) under individual ground motion input are collected from the IDA curves. By assuming a lognormal distribution, fragility curves as demonstrated in Figure 4 can be produced, where the vertical axis is the probability of collapse, i.e. the ductility equals or exceeds 4.0, and the horizontal axis is the intensity ratio (IR). Figure 4 gives an example of fragility curves of the above mentioned Model A, B and C for isolated structures. The IR corresponding to the 50% probability of collapse is taken as the collapse margin ratio (CMR). It is obvious from Figure 4 that CMR decreases significantly from Model A (ideal isolation) to B and C.

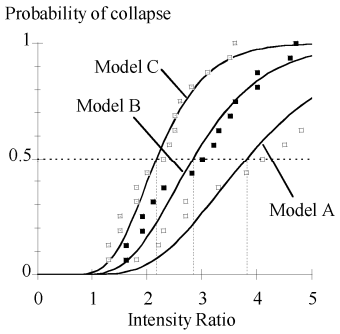

Figure 4 An example of fragility curves of isolated structure

The influences of various parameters on the CMRs of base-isolated structures are discussed. In order to help identifying the sequence of isolator fracture and retaining wall pounding, characteristic deformations (i.e. hardening limit and fracture limit) of the isolator with various total rubber thicknesses nt_R are compared with the size of clearance in Figure 5. For example, if the total rubber thick is 160mm and the clearance is 800mm, the isolator will fracture prior to the pounding. In other words, pounding is not likely to occur in this case.

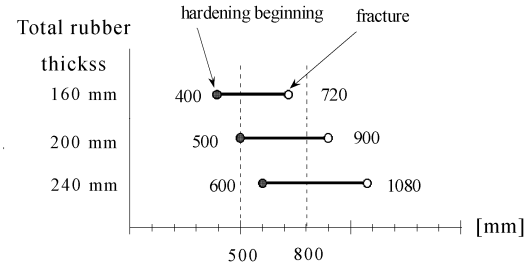

Figure 5 Characteristic deformations of the isolator compared with the size of clearance

Figure 6 summaries the CMRs of the base-isolated structures with various superstructure strengths, total rubber thicknesses, isolation periods, retaining wall properties and sizes of clearance.

For 500mm clearance, as indicated by Figure 5, pounding with the retaining wall occurs prior to the fracture of the isolator and hence dominates the ultimate behavior of the isolated structure no matter the total rubber thickness is 160mm, 200mm or 240mm. In this case, the superstructure strength has only marginal effect on the CMRs, regardless of the total rubber thickness and the isolation period (Figure 6a).

If the retaining wall behaves in an elastic-plastic manner, as shown in Figure 6(b), CMR can be increased considerably with larger superstructure strength, especially when superstructure strength is large enough to resist the shear force in the isolation layer when the retaining wall yields. Meanwhile, larger fracture deformation of the isolator (i.e. larger total rubber thickness) can increase the CMR. Table 1 lists the shear coefficient of the isolation layer when the retaining wall yields in various cases.

Table 1 Shear coefficient of isolation layer when retaining wall yields

Clearance (mm)	Isolation period T_I (s)	Total rubber thickness (mm)		
		160	200	240
500	4.0	0.41	0.39	0.37
	5.0	0.35	0.33	0.32
	6.0	0.31	0.30	0.29
800	4.0	No pounding	0.75	0.52
	5.0		0.56	0.42
	6.0		0.46	0.36

On the other hand, if the clearance of the retaining wall is increased to 800mm, the pounding is not likely to occur since the isolator fractures prematurely if the rubber thickness is only 160mm (See Figure 5). In this case, it makes no difference whether the retaining wall is elastic or elastic-plastic (see Figure 6c and 6d). Otherwise, when the total rubber thickness is 200mm or 240mm, pounding occurs

during the hardening range of the isolator. In these cases, yielding of the retaining wall will permit the isolator to develop larger deformation up to its fracture. As a result, CMR is increased with larger fracture deformation of the isolator (Figure 6d).

It's also worth noting that the CMRs with 800mm clearance are generally larger than those with 500mm clearance.

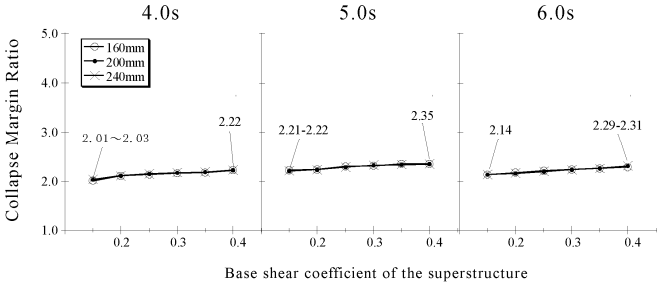

(a) Elastic retaining wall with 500mm clearance

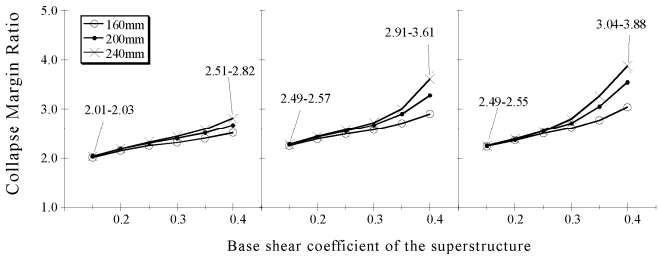

(b) Elastic-plastic retaining wall with 500mm clearance

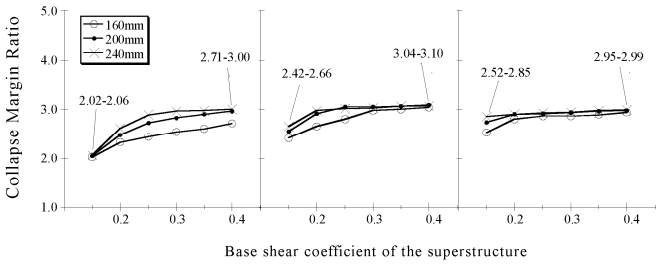

(c) Elastic retaining wall with 800mm clearance

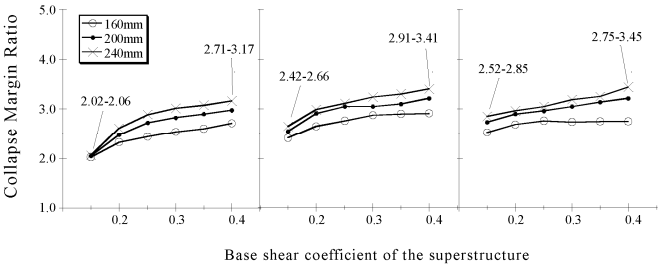

(d) Elastic-plastic retaining wall with 800mm clearance

Figure 6 Influence of various parameters on CMR of base-isolated structures

Figure 7 shows the variations of CMRs of the isolated structure with 5.0s isolation period and 200mm total rubber thickness. If the structure is ideally isolated (i.e. neither pounding nor isolator's nonlinearity is considered), CMR is large and increases dramatically with higher superstructure strength. But this is not realistic. If the clearance is not adequate (say 500mm) and the retaining wall is very strong, CMRs become much smaller and keeps almost constant regardless of the superstructure strength. Yielding of the retaining wall in this case will increase the CMR with the assistance of stronger superstructure. On the other hand, the CMR can be significantly increased if the clearance is enlarged from 500mm to 800mm.

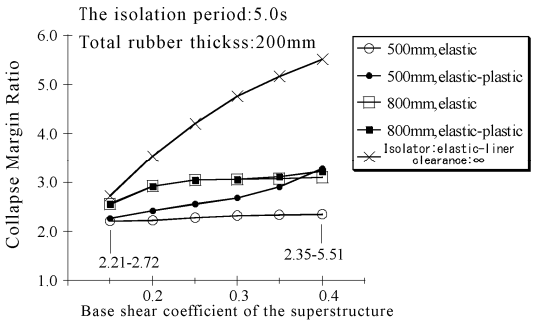

Figure 7 Influence of retaining wall behavior, superstructure strength and clearance size

6. CONCLUSIONS

As a fundamental study on the ultimate state of seismic isolated structure subjected to unexpected strong earthquakes, the seismic performance of base-isolated structures is assessed by incremental dynamic analysis of a 2DOF model with one directional ground motion input. Collapse margin ratios of the models with various influencing parameters are evaluated. From the above discussions, the following conclusions can be drawn:

(1) The seismic safety margin of the base-isolated structures can be significantly increased by increasing the clearance to the retaining walls.

(2) Increasing the strength of superstructure has marginal effect on the overall seismic safety of the base-isolated structure if pounding with the retaining wall occurs and the retaining wall would not yield.

(3) If the retaining wall is appropriately proportioned so that the yielding of retaining wall is prior to that of the superstructure, the seismic safety of base-isolated buildings can be considerable enhanced.

Note that these conclusions are based on the many assumptions made in this study. They should be carefully interpreted in cases where, for example, the higher modes of the superstructure, the vertical failure of the isolator, or the bi-directional ground motion input needs to be considers. These outline the scope of the future study.

References:

Kikuchi, M., Tamura, K. and Wada, A. (1995), "Safety evaluation of base-isolated structures," *J. Struct. Constr. Eng., AIJ*, 470, 65-73.

Kitamura, S., Morishita, M., Yabana, S. and Hirata, K. (2009), "Ultimate behavior tests of seismic isolation system for FBR with A large shaking table (Part1～6)." *Summaries of Technical Papers of Annual Meeting, AIJ*, B-2, 1063-1074.

Vamvatsikos, D. and Cornell, C.A. (2002), "Incremental dynamic

analysis." *Earthquake Engineering and Structural Dynamics*, **31**(3), 491- 514.

FEMA P695 (2009), "Quantification of building seismic performance factors." Federal Emergency Management Agency, Washington, D.C.

Takeda, T., Sozen, M.A. and Nielsen, N.N. (1970), "Reinforced concrete response to Simulated Earthquakes." *Journal Structural Division, ASCE*, **96**(ST12)，2257-2573.

Takayama, M. (1995), "Ultimate capacity of natural rubber bearings used in seismic isolation system." *Journal of Technical Des*., *AIJ*, 1, 160-165.

Yabana, S., Ohtori, Y., Hirata, K., Yasui, K. and Mazda, T. (1996), "Study on linear limits of rubber bearings (Part1 and Part2)," *Summaries of Technical Papers of Annual Meeting, AIJ*, B-2, 691-694.

Uryu, M., Nakayama, K. and Takayama, M. (1996), "Experimental study on natural rubber bearings under high vertical load for base isolation system (Part5)." *Summaries of Technical Papers of Annual Meeting,AIJ*, B-2, 705-706.

JSSI (1995), "Introduction to base-isolated structures." The Japan Society of Seismic Isolation, Ohmusha, 69-71.

Kashiwa, H., Nakayasu, N. and Nakashima, M., (2005). "Response and damage of base-isolated buildings subjected to very varge earthquakes." *Journal of Structural Engineering*, *AIJ*, 51B, 237-246.

Akiyama, H. (1980). "Earthquake-resistant limit-state design for buildings", The University of Tokyo.

BCJ (2005). "Commentary and design examples for the earthquake-resistant design based on energy balance." The Building Center of Japan.

Appendix: Ground motion record set used in the study

Table A1 lists the details of all the 16 ground motion records that are used in this study. These ground motion data are obtain from the PEER/NGA database and the data in Table A1 are also from the database with the exception of the last 3 columns. In these columns, the PGV_{MV} defined in this study and the rotating angles where the PGV_{MV} occurs are listed. These angles are with respect to the 1st component of the original record. In the last column, the normalization factors in accordance with the normalization method in this study are given.

Table A1 Details of the input ground motion records

ID No. (FEMA)	Recording Data					Original Data					Rotated Data		
	Date	Name (Country)	Recording Staion	Epicentral [km]	Magnitude	Component	Lowest Usable Freq [Hz]	PGA [cm/s^2]	PGV [cm/s]	Duration [sec]	PGV_{MV} [cm/s]	θ	*NMi*
2	1994/01/17	Northridge (USA)	Canyon Country-WLC	26.5	6.7	LOS000	0.06	402.11	42.98	20.48	56.88	127°	0.85
						LOS270	0.13	472.68	45.37				
3	1999/11/12	Duzce (Turkey)	Bolu	41.3	7.1	BOL000	0.06	713.50	56.44	81.92	63.69	73°	0.76
						BOL090	0.06	806.50	62.07				
4	1999/10/16	Hector Mine (USA)	Hector	26.5	7.1	HEC000	0.03	260.44	28.56	81.92	44.16	109°	1.09
						HEC090	0.04	330.25	41.72				
5	1979/10/15	Imperial Valley (USA)	Delta	33.7	6.5	H-DLT262	0.06	233.16	25.98	163.84	33.76	103°	1.43
						H-DLT352	0.06	344.32	32.99				
7	1995/01/16	Kobe (Japan)	Nishi-Akashi	8.7	6.9	NIS000	0.13	499.48	37.27	40.96	38.52	109°	1.25
						NIS090	0.13	493.02	36.65				
8	1995/01/16	Kobe (Japan)	Shin-Osaka	46.0	6.9	SHI000	0.13	238.53	37.84	40.96	44.20	31°	1.09
						SHI090	0.10	207.82	27.92				
10	1999/08/17	Kocaeli (Turkey)	Arcelik	53.7	7.5	ARC000	0.09	214.60	17.68	40.96	42.70	66°	1.13
						ARC090	0.05	147.00	39.53				
11	1992/06/28	Landers (USA)	Yermo Fire Station	86.0	7.3	YER270	0.07	344.53	51.40	81.92	56.47	156°	0.86
						YER360	0.07	240.07	29.69				
12	1992/06/28	Landers (USA)	Coolwater	82.1	7.3	CLW-LN	0.13	277.35	25.62	40.96	42.50	84°	1.14
						CLW-TR	0.13	408.82	42.30				
14	1989/10/18	Loma Prieta (USA)	Gilroy Array #3	31.4	6.9	G03000	0.13	544.28	35.67	40.96	49.71	45°	0.97
						G03090	0.13	360.25	44.63				
15	1990/06/20	Manjil (Iran)	Abbar	40.4	7.4	ABBAR-L	0.13	504.61	43.21	81.92	54.92	129°	0.88
						ABBAR-T	0.13	486.75	54.06				
16	1987/11/24	Superstition Hills (USA)	El Centro Imp. Co.	35.8	6.5	B-ICC000	0.13	350.93	46.31	40.96	52.42	28°	0.92
						B-ICC090	0.13	253.33	40.83				
18	1992/04/25	Cape Mendocino (USA)	Rio Dell Overpass	22.7	7.0	RIO270	0.07	377.96	43.78	40.96	51.57	37°	0.94
						RIO360	0.07	538.31	42.04				
19	1999/09/20	Chi-Chi (Taiwan)	CHY101	32.0	7.6	CHY101-E	0.04	346.06	70.59	81.92	115.01	89°	0.42
						CHY101-N	0.05	431.59	114.92				
20			TCU045	77.5	7.6	TCU045-E	0.03	465.17	36.67	81.92	46.96	124°	1.03
						TCY045-N	0.05	502.11	39.07				
22	1976/05/6	Friuli (Italy)	Tolmezzo	20.2	6.6	A-TMZ000	0.13	344.53	22.02	40.96	31.02	82°	1.56
						A-TMZ270	0.13	308.72	30.78				